Properties of gas-atomized Cu-Ti-based metallic glass powders for additive manufacturing

Article *in* Materials and Design · March 2022

DOI: 10.1016/j.matdes.2022.110519

9 authors, including:

E. Soares Barreto
Universität Bremen
6 PUBLICATIONS **50** CITATIONS
SEE PROFILE

Maximilian Frey
Universität des Saarlandes
22 PUBLICATIONS **118** CITATIONS
SEE PROFILE

Jan Wegner
University of Duisburg-Essen
11 PUBLICATIONS **54** CITATIONS
SEE PROFILE

Allen Jose
Universität Bremen
1 PUBLICATION **0** CITATIONS
SEE PROFILE

Materials & Design 215 (2022) 110519

Contents lists available at ScienceDirect

Materials & Design

journal homepage: www.elsevier.com/locate/matdes

Properties of gas-atomized Cu-Ti-based metallic glass powders for additive manufacturing

Erika Soares Barreto [a,e,*], Maximilian Frey [b], Jan Wegner [c], Allen Jose [a], Nico Neuber [b], Ralf Busch [b], Stefan Kleszczynski [c,d], Lutz Mädler [a,e], Volker Uhlenwinkel [a,e]

[a] Leibniz Institute for Materials Engineering—IWT, Badgasteiner Str. 3, 28359 Bremen, Germany
[b] Chair of Metallic Materials, Saarland University, Campus C6.3, 66123 Saarbrücken, Germany
[c] Chair of Manufacturing Technology, University Duisburg-Essen, 47057 Duisburg, Lotharstr. 1, Germany
[d] Center for Nanointegration Duisburg-Essen (CENIDE), 47057 Duisburg, Carl-Benz-Str. 199, Germany
[e] Faculty of Production Engineering, Particle and Process Engineering, University of Bremen, Badgasteiner Str. 1, 28359 Bremen, Germany

HIGHLIGHTS

- Fully amorphous powders of Cu-Ti-based glass-forming alloys are obtained from gas-atomizing single elements with industrial-grade purities.
- The amorphous solidification of the powder indicates a suitable GFA for processing Cu-Ti-based metallic glasses via additive manufacturing.
- The oxygen uptake during atomization is a function of particle size, governed by the surface-to-volume ratio of droplets.
- The increase of atomization gas pressure produces finer particles and a positive consequence is the increased powder yield in the range of 20–63 μm.
- The powders produced are highly spherical with desired flowability for additive manufacturing.

GRAPHICAL ABSTRACT

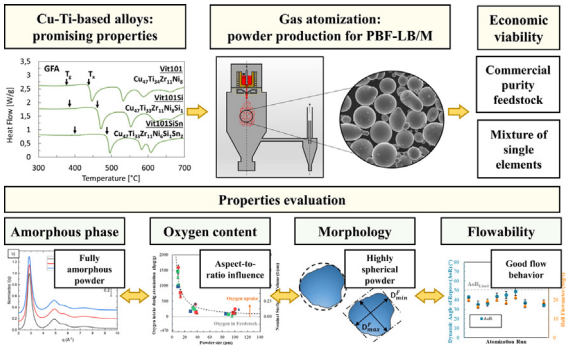

ARTICLE INFO

Article history:
Received 8 December 2021
Revised 28 February 2022
Accepted 3 March 2022
Available online 8 March 2022

Keywords:
Metallic glasses
Gas-atomization

ABSTRACT

Laser powder bed fusion (PBF-LB/M) of bulk metallic glasses permits large and complex components to solidify to an amorphous state, thus expanding the processing possibilities of this material class. Here, the Cu-Ti-Zr-Ni family, also known as Vitreloy 101, is systematically investigated for processing of the PBF-LB/M powder itself. Gas atomization was used to produce powder of Vit101 and derivates micro-alloyed with Si and Sn. The influence of atomization and alloy composition on glass formation, oxygen content, particle morphology, and flowability were investigated. Amorphous powder was successfully obtained using industrial-grade purity as feedstock for the atomization. The oxygen content within the powder was controlled by the surface-to-volume ratio, without significant influence of the different atomization parameters and the microalloying itself. The powder displayed high circularity with sufficient flowability

* Corresponding author at: Leibniz Institute for Materials Engineering—IWT, Badgasteiner Str. 3, 28359 Bremen, Germany.
E-mail address: uhl@iwt.uni-bremen.de (E. Soares Barreto).

https://doi.org/10.1016/j.matdes.2022.110519

Powder properties
Oxygen contamination
Laser-based powder bed fusion of Metals (PBF-LB/M)
Vitreloy 101

after drying. Our results contribute to the investigation of Vitreloy 101 alloys as promising candidates for PBF-LB/M applications.

1. Introduction

Additive manufacturing (AM), especially laser powder bed fusion (PBF-LB/M), is recently widely investigated for the synthesis of components made of bulk metallic glasses (BMGs). The cooling rates of the melt pool reach up to 10^6 Ks^{-1} during PBF-LB/M [1], theoretically far beyond the ones required to bypass crystallization and generate the amorphous phase in BMGs [2]. Therefore, the layer-wise manufacturing approach allows the size and geometry of parts to be decoupled from the typically critical diameter d_c of conventional casting technologies. Nonetheless, (nano-) crystallization, porosity, and embrittlement remain challenges in the additive manufacturing of BMGs.

So far, Zr-based are among the most investigated glass-forming systems for PBF-LB/M due to their high glass-forming ability and fracture toughness [2]. However, the Cu-Ti-Zr-Ni family is a promising alternative as it contains economically interesting starting materials and high strength with a reasonable glass-forming ability (GFA) [3–7]. The quaternary composition found to possess the highest GFA is $Cu_{47}Ti_{34}Zr_{11}Ni_8$, also known as Vitreloy 101 [4,8]. The critical cooling rate (CCR) required for vitrification is approximately 250 Ks^{-1} [5,7,8]. Microalloying with Si and Sn leads to the destabilization of oxides that act as nucleation sites, which improves the thermal stability of the supercooled liquid region, ΔT_x [3–7], between the glass transition and the onset of crystallization upon heating. As a direct consequence, the reduction of the CCR is reported to decrease by at least a factor of three [3]. In this context, the compositions found with the highest GFA were $Cu_{47}Ti_{33}Zr_{11}Ni_8Si_1$ [3,9] and $Cu_{47}Ti_{33}Zr_{11}Ni_6Sn_2Si_1$ [6]. Nonetheless, the properties of these alloys after laboratory casting are not necessarily transferable to industrial gas-atomized powders (feedstock for PBF-LB/M). Their characteristics will therefore be investigated and reviewed given their qualification for the PBF-LB/M fabrication.

The initial powder properties play a crucial role in PBF-LB/M processability. Sufficient powder flowability is necessary to create good-quality layers during recoating. The layer properties are directly related to part quality and low-defect fabrication. There is a tendency to use fine and spherical powder as they show better flowability and spreadability [10,11]. However, the interparticle forces such as the Van-der-Waals attractive forces can exceed the gravitational forces, especially for smaller particles, which leads to powder cohesion and lack of flowability [12–14]. Gas atomization parameters can, to some extent, tailor droplet formation. The most frequent method to influence the mean particle size is to vary the atomization gas pressure [15]. In general, increased pressures yield finer particles, which typically have higher circularity than coarser ones. Another example is the use of hot gas atomization. It reduces gas consumption and produces a larger fraction of smaller particles. For particles with a smaller diameter, the amorphous fraction is higher and therefore the amorphous yield significantly increases in the case of glass-forming systems [16,17].

BMG powder contains higher oxygen contents than comparable cast materials. In Zr-based BMGs, this usually leads to a lowered GFA [18–21], requiring higher cooling rates to form fully amorphous parts and increased chance of (nano-)crystallization during thermal cycling in PBF-LB/M processing [22,23]. The negative impact of oxygen has been mostly investigated in Zr-based glass-formers [2,22–27]. For instance, Wegner et al. [26] reported an extremely narrowed process window for the AMZ4 alloy (in at.% $Zr_{59.3}Cu_{28.8}Al_{10.4}Nb_{1.5}$) with higher oxygen levels in which high-quality, amorphous parts are manufactured via PBF-LB/M. The increased oxygen content drastically compromised flexural strength [26]. Frey et al. [27] attributed the absence of ductility in an additively manufactured AMZ4 alloy to the high oxygen contamination. This further points out the importance to monitor and understand the oxygen uptake during the entire processing chain from powder production until the final additively manufactured component. Due to the high affinity of Zr-based BMGs to oxygen [18,25], expensive high purity materials instead of commercial purity (industrial-grade) are typically required. Nevertheless, glass-formers that rely on the high purity of the feedstock are costly and their commercial availability is constrained. Thus, the investigation of Cu-Ti-based glass-forming systems is attractive for PBF-LB/M manufacturing, as the affinity of copper to oxygen is lower. Therefore, this could represent advantages from the material feedstock selection until the AM production of components with an expected smaller oxygen content.

The present work evaluates the gas-atomization process and the resulting physical, structural and chemical properties of the Cu-Ti-Zr-Ni family for laser additive manufacturing applications. The compositions $Cu_{47}Ti_{34}Zr_{11}Ni_8$ (Vit101), $Cu_{47}Ti_{33}Zr_{11}Ni_8Si_1$ (Vit101Si), and $Cu_{47}Ti_{33}Zr_{11}Ni_6Sn_2Si_1$ (Vit101SiSn) were investigated. Feedstock materials using single elements with commercial purity were used for gas atomization in view of the economic viability at industrial scales. In total, each alloy was gas-atomized three times by investigating the gas pressure and gas temperature in each run, aiming for vitrification and a higher yield in the 20–63 μm class size. The formation of an amorphous state, oxygen content, particle morphology, and flow behavior were investigated.

2. Materials and methods

2.1. Powder synthesis

The Vit101, Vit101Si, and Vit101SiSn glass-forming alloys were atomized with a close-coupled gas atomizer (CCA) (more details in Ref. [16]). Table 1 displays the feedstock materials comprised of commercial purity (CP) elements (Ti, Zr, Ni, Sn, and Si) and CuNi (3.6 wt% Ni) pre-alloy. The alloys were obtained by proportionally mixing the elements to achieve the desired chemical composition. This eliminates the need for pre-casting into master alloys and promotes higher cost-effectiveness of the process. High purity

Table 1
Degree of purity of the feedstock material used for the gas-atomization of the Vitreloy 101 alloys.

Alloy	Purity
CuNi (3.6 wt% Ni)	99.95%
Ti	99.4%
Zr 702	99.2%
Ni	99.8%
Sn	99.98%
Si	99.99%

(<20 ppm impurities) graphite crucibles treated via halogen purification (2120PT, Mersen) were used to prevent reactions and the uptake of impurities. The atomization tower was purged with Argon (purity $\geq$ 99.996%) to reduce the oxygen content. The Argon was also used as the processing gas. A nozzle of 2 mm diameter was selected. The melt was superheated to a temperature of 1673 K and held for 7 min before removing the stopper rod to start the atomization process. The impingement of the high-velocity gas stream disintegrated the melt flow into droplets. The droplets solidified during flight inside the atomization tower and were collected at the bottom.

Three series of atomization runs were conducted for each alloy. The first atomization was performed using gas at room temperature (RT) at a pressure of 1.2 MPa (p1.2,RT). For the second atomization, the gas pressure was raised to 1.6 MPa and kept at RT (p1.6,RT). Finally, the last atomization was conducted with a gas pressure of 1.6 MPa and hot gas (HG) at 593 K (p1.6,HG). Table 2 summarizes the main atomization parameters, including the results for gas-to-melt mass flow ratio (GMR), mass median particle diameter ($d_{50,3}$) obtained with a laser diffraction instrument with wet dispersion (Malvern Mastersizer 2000), and the geometric standard deviation σ_G calculated according to $\sigma_G = (d_{84,3}/d_{16,3})^{0.5}$.

2.2. Powder characterization

The synthesized powder was initially sieved below 250 μm aperture to remove splats and flakes from the atomization process. The fine particles (approx. < 20 μm) were removed with an air classifier (Multiprocess system 50 ATP, Hosokawa Alpine). To reduce chances of oxidation or contamination, the classification was performed under inert atmosphere using nitrogen for the separation. In sequence, the powder was sieved below 63 μm to separate coarser particles. The exception was the Vit101SiSn alloy atomized with hot gas at a pressure of 1.6 MPa, in which only sieving was used for the classification due to a reduced powder amount.

Scanning electron microscopy (SEM) images were acquired with a TESCAN VEGA II XLH. The chemical composition of the powders was measured with an energy dispersive X-ray analysis detector (EDX) coupled to the SEM.

The particle shape factors of circularity and aspect ratio were determined with the measuring principle of static image analysis (Morphologi G3, Malvern Panalytical). In the static mode, the dry powder is dispersed over an object slide and high-quality images of every particle are captured over a defined area. The factors are dimensionless and have a value of 1 for ideal spherical particles. Therefore, the larger the calculated values, the more spherical the shape of the particle. While circularity is defined as the ratio between the perimeter of an equivalent circle with the same area as the particle divided by the perimeter of the actual particle, the aspect ratio represents the elongation of the particle and is a measurement of the width-to-length ratio. The results were averaged over two measurements per sample with at least 10^5 particles in total.

Powder flowability was measured with a Hall Flowmeter funnel of 2.5 mm aperture as stated in DIN EN ISO 4490 and with a dynamic flow test (angle of repose of at least ten images) using a self-designed device (more details in Ref. [14]). Before the measurements, the powders were kept in a desiccator for at least 24 h to reduce the moisture content.

Furthermore, the crystallinity measures were evaluated with X-ray diffraction (XRD, PANalytical X'Pert Pro diffractometer) between the angles (2θ) of 20° to 80° using Cu-Kα radiation with a wavelength of 1.5406 Å. Complementary, the powder fraction 20–63 μm was measured with high energy Ssynchrotron X-ray diffraction (HESXRD) performed in transmission mode at room temperature at the P21.2 beamline of PETRA III of the Deutsche Elektronen-Synchrotron (DESY) in a wavevector range Q from 2 to 10 $Å^{-1}$. A wavelength of 0.177138 Å (70 keV) was used with a VAREX XRD4343CT detector (2880 × 2880 pixels) to record the two-dimensional diffraction pattern, which was further integrated using PyFAI and then processed with the PDFgetX2 software [28] to obtain the background-corrected scattering intensity I(Q).

Thermal properties of the powders were studied by differential scanning calorimetry (DSC). Heating scans with 1 Ks^{-1} rate from 550 °C to 850 °C were performed using a Perkin-Elmer DSC 8000 under high-purity Argon flow. The powder samples were encapsulated in Aluminum pans.

The oxygen content of the powders was measured with hot gas extraction (ELTRA ONH-2000) for each class size for samples of ca. 50 mg using helium (99.999%) as the carrier gas. The results were averaged from three measurements. The concentration of oxygen in the spray chamber before the beginning of the atomization was analyzed with an O_2 Analyzer from Bailey Fischer Porter.

3. Results and discussion

3.1. Physical properties

The particle size distribution of the powders was investigated with laser diffraction. The complete results are given in Fig. A1 (s. Appendix) and exemplary results are depicted in Fig. 1. The distribution density q_3 presents the probability of a particle with diameter d to be found in the population, whereas the cumulative mass distribution Q_3 indicates the percentage of undersized or oversized particles than a specific diameter d. Commonly, the mass

Table 2
Process conditions of the melt atomization.

Run	Alloy	p (MPa)	T_{gas} (K)	Inert Gas	D (mm)	ΔT_m (K)	$\dot{m}_G$ (kg/h)	$\dot{m}_L$ (kg/h)	GMR (–)	$d_{50,3}$ (μm)	σ_G (–)
1	Vit101							149	4.0	52	1.9
	Vit101Si	1.2	293 (RT)	Argon	2	~500	592	150	4.0	50	2.2
	Vit101SiSn							150	3.9	47	2.5
2	Vit101		293 (RT)					133	5.9	40	2.1
	Vit101Si	**1.6**		Argon	2	~500	780	172	4.5	45	2.4
	Vit101SiSn							141	5.6	33*	2.1
3	Vit101							153	3.4	33	2.4
	Vit101Si	**1.6**	**593 (HG)**	Argon	2	~500	513	155	3.3	35	2.5
	Vit101SiSn							143	3.6	26*	2.7

Vit101 = $Cu_{47}Ti_{34}Zr_{11}Ni_8$, *Vit101Si* = $Cu_{47}Ti_{33}Zr_{11}Ni_8Si_1$, *Vit101SiSn* = $Cu_{47}Ti_{33}Zr_{11}Ni_6Sn_2Si_1$, p = Atomization gas pressure, T_{gas} = Initial gas temperature, D = Nozzle outlet diameter, ΔT_m = Superheated melt temperature, $\dot{m}_G$ = Gas mass flow rate, $\dot{m}_L$ = Melt mass flow rate, *GMR* = Gas-to-melt mass flow ratio, $d_{50,3}$ = Mass median particle diameter, σ_G = Geometric standard deviation, RT = Atomization gas at ambient temperature, HG = Hot gas atomization.
* Powders self-ignited after gas-atomization and led to material losses, thus interfering with the results for $d_{50,3}$.

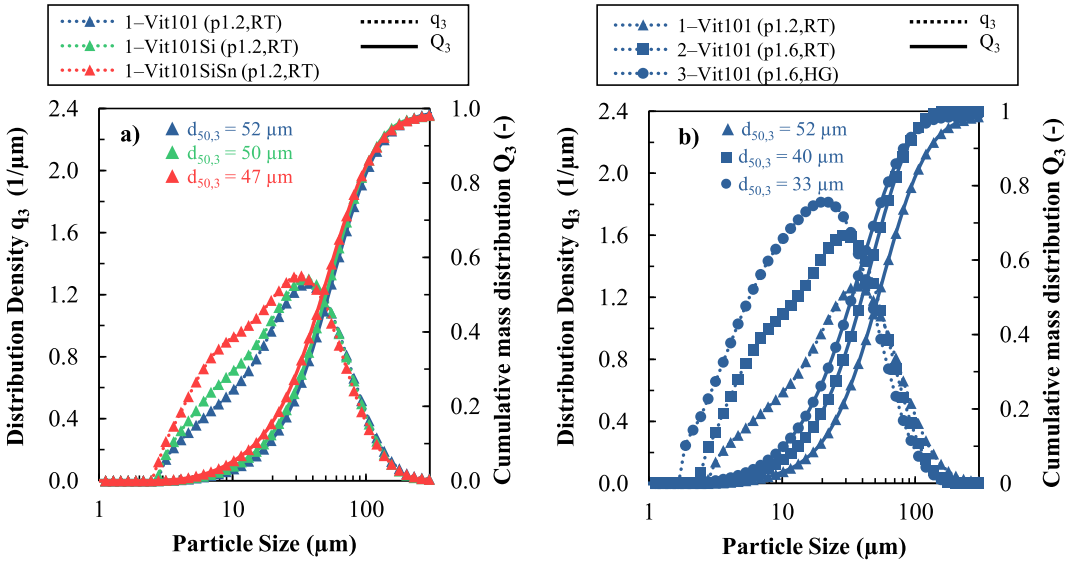

Fig. 1. Distribution density q_3 and cumulative mass distribution Q_3 as a function of particle size, including $d_{50,3}$, for (**a**) Vit101, Vit101Si, and Vit101SiSn powders atomized in the first atomization run, showing the small impact of alloy composition during gas-atomization; (**b**) Vit101 powders atomized using different atomization conditions, displaying the influence of gas pressure and temperature on droplet formation.

median particle diameter $d_{50,3}$ is used to represent the averaged particle size of the distribution. Fig. 1 (a) shows the influence of alloy composition on the particle distribution (0–250 µm) atomized with gas at room temperature at a pressure of 1.2 MPa. Similar cumulative mass distributions were obtained. Microalloying slightly decreased the $d_{50,3}$, therefore only a weak correlation based on alloy composition can be deducted.

Fig. 1 (b) exemplarily compares the influence of gas pressure and gas temperature on the particle size distribution of the Vit101 alloy. Finer particles were generated at higher gas pressure and gas temperature, as the $d_{50,3}$ changed from 52 µm in the first atomization run, to 40 µm and 33 µm in the second and third atomization runs, respectively. Moreover, the distribution density curve was shifted to smaller particles. It is known that the gas properties control the gas mass flow rate according to the well-known empirical correlation to predict $d_{50,3}$ proposed by Lubanska [29]. As expected, the increase in gas pressure resulted in smaller particle sizes caused by the higher gas melt flow ratio and consequently GMR. Likewise, the results confirmed hot gas atomization enables the synthesis of smaller particles. Despite the lower gas melt flow ratio caused by the increased gas density at higher temperatures, the kinetic energy and gas velocity are raised, which is inversely proportional to $d_{50,3}$ [16]. Therefore, smaller particles are obtained with hot gas atomization.

One advantage of reducing the mean particle diameter and consequently the shift of the curve to smaller particle sizes was the mass yield of the 20–63 µm fraction. For the initial set of atomization parameters (gas at room temperature at a pressure of 1.2 MPa), the average yield was 50 ± 1% after classification. Increasing gas pressure and temperature increased the powder yield to 55 ± 3%, although a higher fraction of fine particles below 20 µm was generated in the latter. Increasing the usable fraction of powder is associated with costs reduction, better usage of resources (e.g., material feedstock, gas, crucible, others), and energy-saving, resulting in better efficiency of the powder metallurgy production chain [30].

Fig. 2 presents SEM micrographs of the 20–63 µm powder. The particles exhibited a spherical shape and relatively smooth surface topography. With hot gas atomization, an increased number of satellites is observed. Satellites are smaller particles that solidify faster and collide in flight with larger semi-solid ones, remaining attached and forming aggregates [13,24]. Comparable results for Fe-based and Zr-based glass-forming alloys have been observed by Ciftci et al. [31].

The presence of satellites and the building of aggregates has been reported to reduce the circularity of powders [13] and deteriorate powder flow properties [32]. This higher particle flow resistance is normally attributed to mechanical interlocking caused by irregularities and the dominance of interparticle forces as Vander-Waals in satellites [32]. As previously seen in Fig. 1 (b), the combination of hot gas atomization and high gas pressure considerably raised the formation of smaller particles. Although the host particles remained spherical (circularity close to 1), the results suggested a larger fraction of irregular particles.

Moreover, elongated particles with an aspect ratio smaller than 0.25 (AR $\leq$ 0.25) were observed using gas at room temperature at a pressure of 1.2 MPa, as indicated in Fig. 2 (a, c). These particles solidify into ligaments after the disintegration of the melt stream, but before completion of the spheroidization process [33]. This is characteristic of the atomization of melts with high viscosity, generally the case for BMG-forming liquids such as the present Cu-Ti-based compositions [3,8,34,35]. The hot gas atomization can increase the spheroidization time of ligaments and help to prevent the formation of fiber-like particles for high-viscous melts [33,36]. The reason is the reduced temperature gradient between the hot gas and melt jet during atomization, resulting in a lower heat transfer rate. This extends the time frame in which the melt droplets stay in a state of low viscosity, which permits spherical particles to form due to the surface tension in the spray [33].

Fig. 3 displays the measured results for the particle shape factors. The range from 20 µm to 60 µm was chosen based on requirements of the AM processing [2,12]. The circularity and aspect ratio of the powders were above 0.84 and 0.68, confirming the SEM observations of spherical particles. While the lowest particle shape factors were measured for Vit101Si, the Vit101SiSn powders presented the most spherical form. AMZ4 powder gas-atomized with the same parameters by Ciftci [37] was more irregular, attributed to the higher viscosity of this alloy at the liquidus temperature.

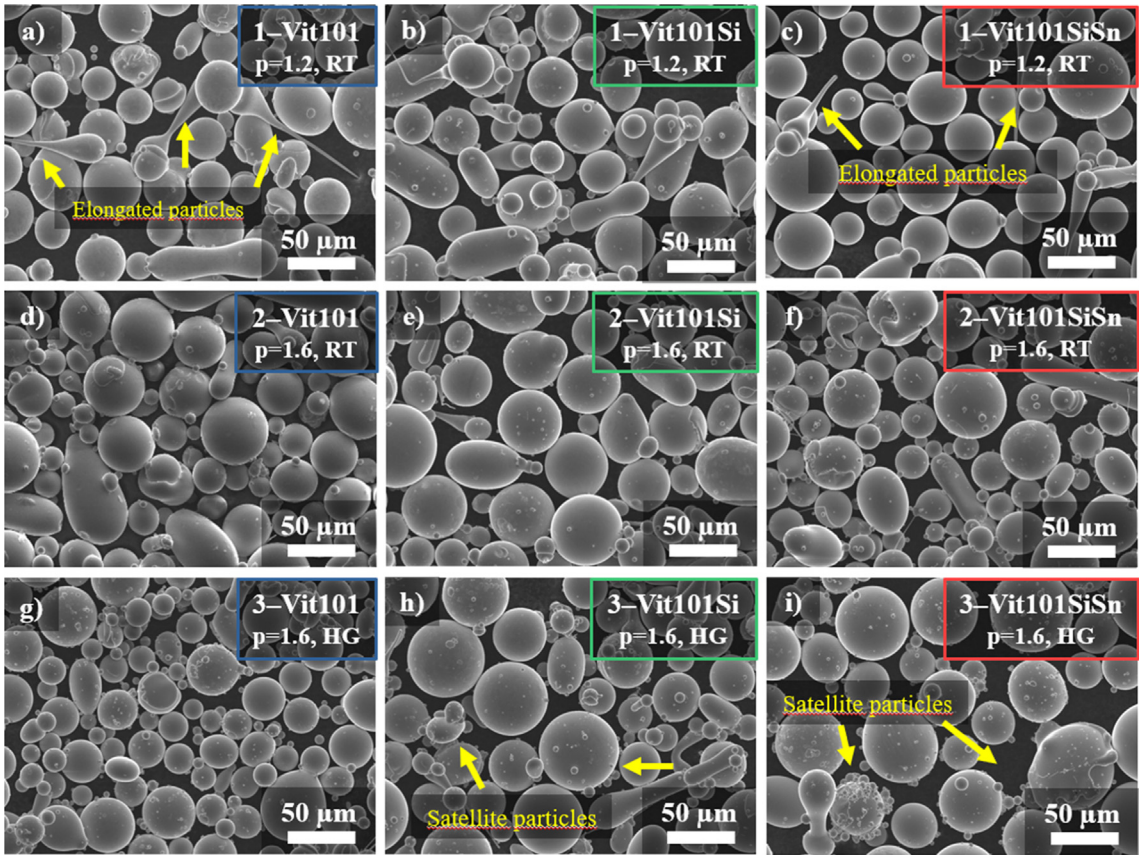

Fig. 2. SEM micrographs of Vit101, Vit101Si, and Vit101SiSn particles (20–63 μm) atomized with (**a-c**) gas at room temperature at a pressure of 1.2 MPa; (**d-f**) gas at room temperature at a pressure of 1.6 MPa; (**g-i**) hot gas at a pressure of 1.6 MPa. The arrows indicate the formation of elongated particles in the first atomization run and satellites in the third run.

The viscosity of Vit101 at the melting point is only about 40% of the viscosity of typical Zr-based alloys such as Vit1, Vit105, Vit106 and AMZ4 [38].

As it can be seen in Fig. 3, coarser particles are more irregular than smaller ones. This result is consistent with previous reports in the literature [13,31,36]. Larger particles require a longer time for the spheroidization process to complete. Hence, they tend to be less spherical than smaller ones. Increasing the gas pressure also seems to have enhanced the formation of more irregular particles.

Regarding the use of hot gas atomization, the results corroborate that the particle shape factors decrease, attributed to the formation of satellites. However, it was argued atomizing with hot gas can contribute to the spheroidization process of high viscous melts, thus preventing the formation of elongated particles. This would, in contrast, contribute to the improvement of particle shape factors.

To evaluate this hypothesis, the fraction of particles with an aspect ratio equal to or inferior to k = 0.25 was quantified in the 20–63 μm range. This threshold value (k) corresponds to elongated particles formed during the atomization of viscous melts, as previously discussed. Fig. 4 displays the results for each alloy according to the parameter used.

The fraction of elongated particles formed during atomization is independent of the atomization process, as none of the differences observed are statistically significant within the parameter selection (Fig. 4). This is indicative of the lack of contribution of HG atomization on particle spheroidization. Instead, the chemical composition plays a major role. While the fraction of particles with AR $\leq$ 0.25 is about 0.7 ± 0.1% for the Vit101, the microalloying with Si increases the fraction to near 1.1 ± 0.1%, and the combined additions of Si and Sn to slightly over 1.31 ± 0.03%, nearly double of the initial base composition. Because the incomplete spheroidization process is strongly related to the viscosity of the alloys, the findings suggest that microalloying causes the melt viscosity to slightly increase. The viscosity of glass-forming alloys is usually associated with the fragility concept, which reflects the sensitivity of the liquid melt to temperature changes [9]. It has been shown in various studies a larger fragility parameter leads to lower the critical cooling rate needed for the melt to freeze into the glassy state [34,35,39–41]. Thus, the sluggish kinetics derived from high viscous melts is a good indication of improved GFA, as the formation of crystalline phases is retarded [39,41]. Venkataraman et al. [9] reported a higher fragility parameter for Vit101Si compared to Vit101, which is in agreement with the higher GFA of this alloy as previously discussed. They also argued that higher fragility parameters for Cu-based glass-formers are fundamentally an indication of reduced CCR. Hence, the fragility of Vit101SiSn should be even higher, as it has the highest GFA of the investigated alloys. Consequently, the melt kinetics should be more sluggish, which would explain the increased fraction of particles with lower aspect ratios resulting from an incomplete spheroidization process.

Taken together, the findings of this study suggest, although changes in viscosity influenced droplet formation, the particle morphology is predominantly controlled by the particle size and presence of satellites. As these factors affect the powder rheology [12,14,42–44], the flowability was investigated next.

Fig. 5 displays the results obtained via dynamic angle of repose and a hall flowmeter. In general, a satisfactory flow behavior for PBF-LB/M applications is obtained, normally associated with an angle of repose inferior to 50°. A direct influence of particle size

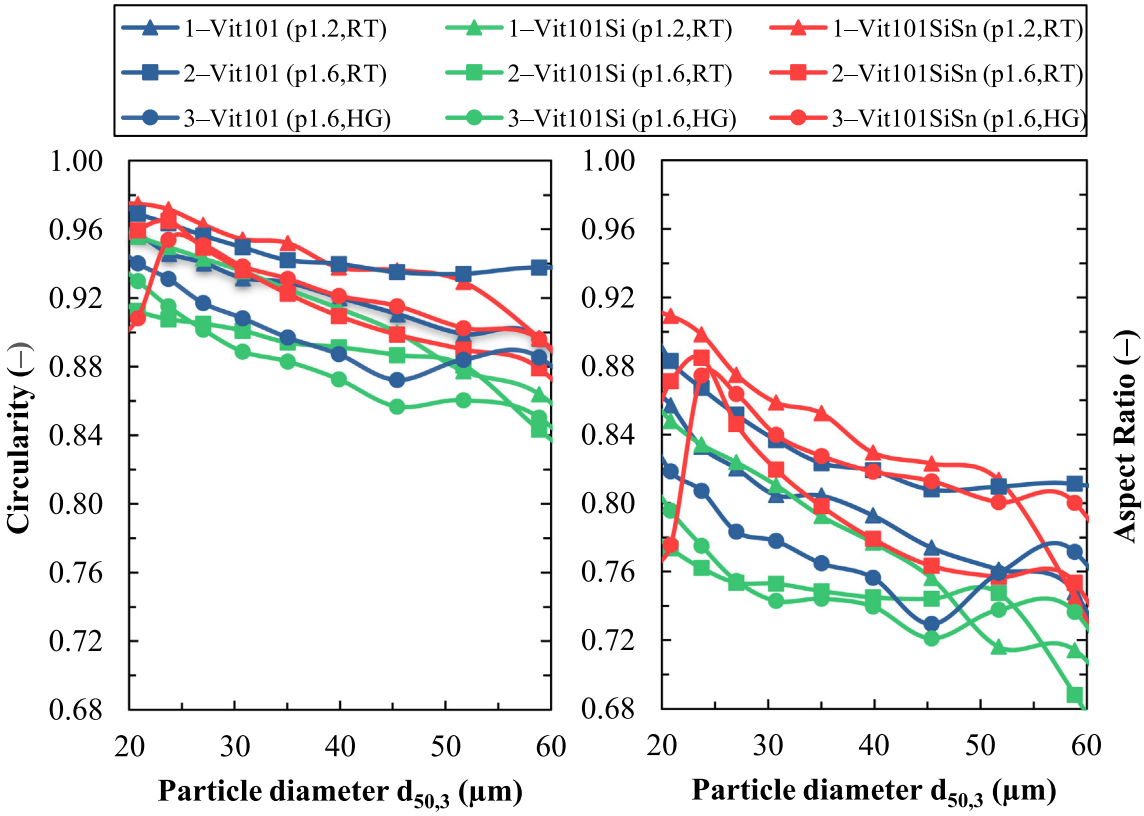

Fig. 3. Circularity and aspect ratio analyses for the gas-atomized Cu-Ti-based glass-forming alloys as a function of particle size, measured by the static image analysis.

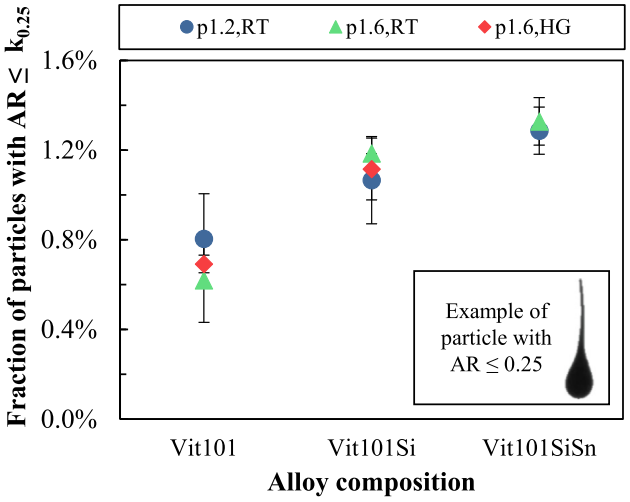

Fig. 4. Fraction of particles with an aspect ratio equal to or smaller than 0.25, according to the alloy composition and gas-atomization run, where *p* = gas pressure in MPa, *RT* = gas at room temperature, and *HG* = hot gas atomization. The insert contains an example of a particle with AR ≤ 0.25.

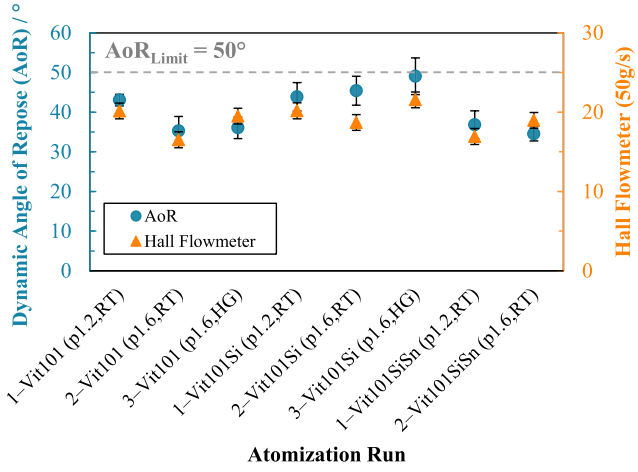

Fig. 5. Flowability of powders (20–63 µm) measured with dynamic angle of repose (AoR) and hall flowmeter.

distribution and morphology on the flowability results is less straightforward, as the results lie within the same range.

The powders seem to be quite prone to moisture uptake, as the flowability quickly worsened after short exposures to the environment. This is particularly observed for the Vit101SiSn powder. It has been reported CuSn surfaces have a higher reactivity than Cu surfaces, as adsorbates are more strongly bound [45]. Our results contribute to the notion that Sn promotes increased reactivity in Cu-Ti-based alloys.

The improper handling and storage of these powders could be detrimental to the additive manufacturability of Vitreloy 101 alloys if the moisture strongly hinders the flowability. This can cause an unsystematic and discontinuous spread of the layered bed, which in turn can favor layer porosity, non-uniform layer density, and increased surface roughness [43,44,46–48]. Consequently, the final product properties and quality is impaired.

3.2. Structural and chemical properties

EDX analyses confirmed the desired chemical composition obtained for the powders (Fig. B1 s. Appendix).

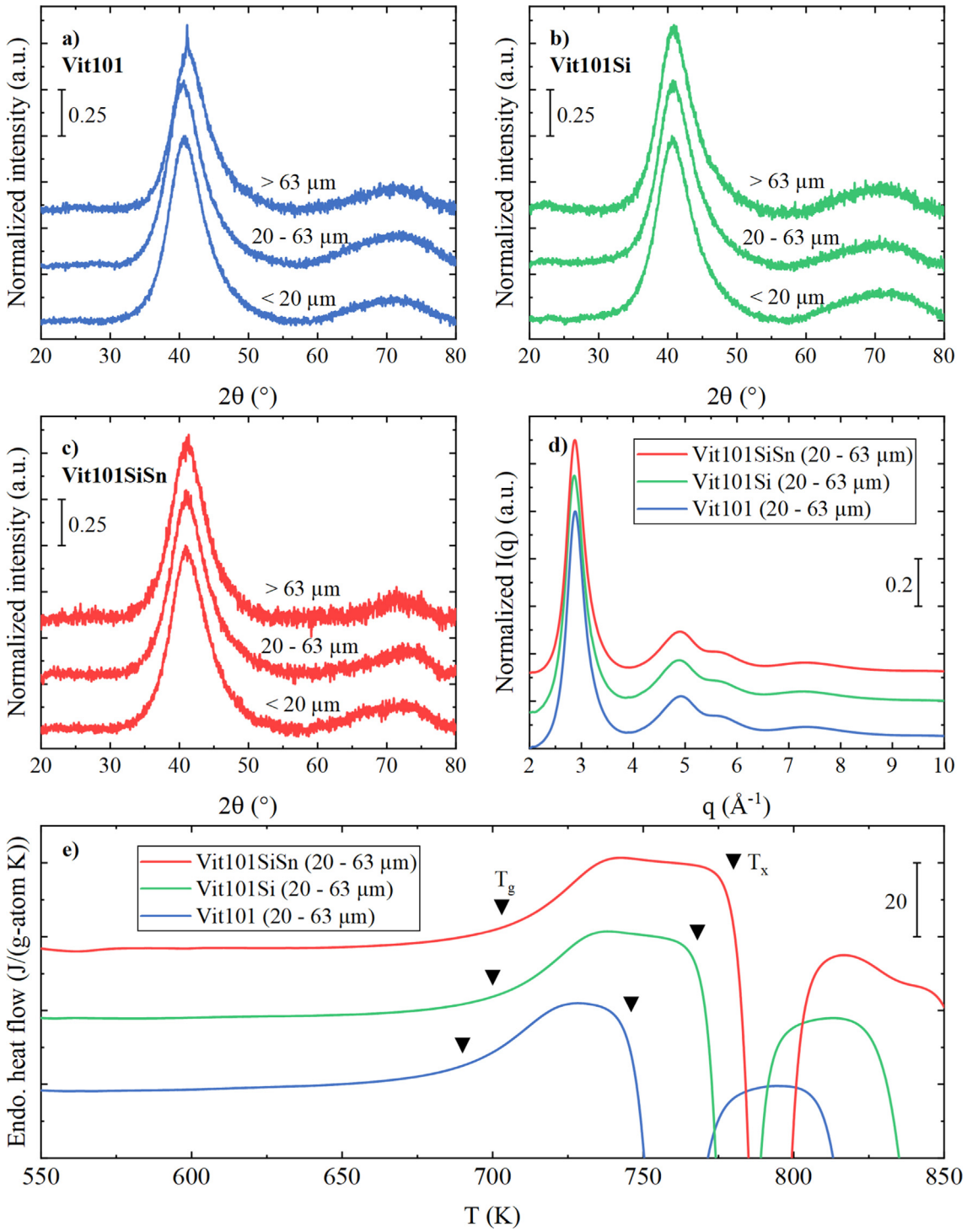

Fig. 6. X-ray diffraction of gas-atomized powders at different class sizes for: (**a**) Vit101; (**b**) Vit101Si; (**c**) Vit101SiSn; (**d**) High-energy Synchrotron (HESXRD) of each alloy of class size 20–63 µm. The investigation was conducted with powders obtained in the first atomization run. The results show the for BMGs typical broad halo, which can be attributed to an amorphous structure. (**e**) DSC scans (1 Ks^{-1}) of all three alloys of the size class 20–63 µm. The thermal stability increases with the increasing addition of alloying elements, as indicated by the length of the supercooled liquid region between the onset of the glass transition, T_g, and the onset of crystallization, T_x.

The influence of microalloying on the powder structure was investigated with X-ray diffraction and the results are illustrated in Fig. 6. The powders exhibited the typical broad halo for BMGs, which can be attributed to an amorphous structure within the detection limits of the method. Small crystalline peaks at approx. 41° were detected only in coarser particles (above 63 µm) of Vi101, which has the lowest GFA of the investigated derivates. As the cooling rate decreases with the increase in particle size [49], the solidification time experienced by the larger droplets during the atomization process seems to be insufficient to completely bypass crystallization. Nonetheless, the relatively weak signal intensity of the reflection implies the crystalline phase is present in small quantities. Similar small-intensity crystallization events in a PBF-LB/M-sample of Vit101SiSn alloy have been reported

and attributed to a Cu_2Ti_4O phase [21]. As particles above 63 μm have less significance to PBF-LB/M applications, a detailed phase analysis was disregarded in this study.

Further analyses on powders with particles in the range of 20–63 μm were performed using high-energy synchrotron X-ray diffraction (HESXRD) (Fig. 6 (d)). With the high energy used for HESXRD in transmission mode, even smaller volumes of crystals can be revealed over the entire volume of the powder particles, offering much greater sensitivity and resolution than conventional laboratory XRD. The results confirmed the broad halo formation typical of amorphous structures, as well as the absence of Bragg reflexes that would indicate crystallites, suggesting the gas-atomized powder was fully amorphous.

The amorphous state in the feedstock powder is nonessential to generating amorphous parts via PBF-LB/M as re-melting and re-heating steps occur in the heat-affected zone. Studies have demonstrated that fully amorphous BMGs have been additively manufactured regardless of the presence of crystallinity in the powder [50]. There are, however, significant advantages in generating amorphous over crystalline powder. The lack of crystallization is linked with improved GFA and lower oxygen contents, which simultaneously broadens the process window for BMGs via PBF-LB/M [2,24,26]. Moreover, considering the overall industrial scope, other subsequent processing routes such as the thermoplastic forming (TPF) necessarily require amorphous powder for amorphous part consolidation [27,51–54]. The TPF process window is associated with the so-called supercooled liquid region, which is the temperature window between the onset of glass transition, T_g, and the onset of crystallization, T_x, in which the deeply supercooled liquid can be processed without crystallization. Hence, there is a general interest in increasing the yield of amorphous powder generated by gas-atomization. In Fig. 6 (e), the DSC scans of all three powders of the size class 20–63 μm are shown. The glass transition events are distinctly visible by an increase of the heat flow, underlining the amorphous character of the powders. The glass transition onset temperatures T_g for Vit101, Vit101Si, and Vit101SiSn slightly differ with 690 K, 700 K, and 703 K, respectively. In contrast, the onset of crystallization T_x, indicated by a distinct exothermal drop in the heat flow signal, shifts considerably by microalloying. It increases from 746 K for the base alloy Vit101 to 768 K through the minor addition of Si and up to 780 K for the Vit101SiSn alloy. Thus, the micro-alloyed systems feature distinctly increased thermal stability against crystallization, as previously reported in [7]. For TPF applications, this goes hand in hand with a broader processing window and, hence, better deformability [52].

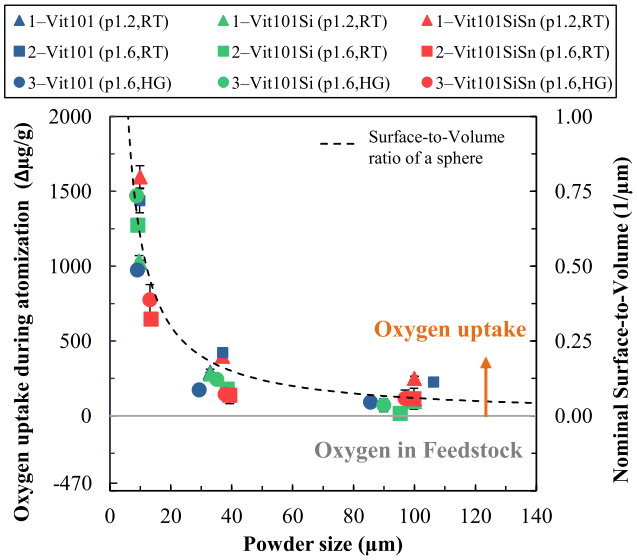

Fig. 7. Oxygen uptake during atomization of Vit101, Vit101Si and Vit101SiSn alloys as a function of the particle size. The oxygen uptake was dominated by the surface-to-volume ratio of a sphere.

According to Ciftci et al. [49], the cooling rate experienced by the particle class size of 20–63 μm during gas-atomization varies from 10^3 to 10^4 Ks^{-1}. Thereby, the present cooling rates experienced in the process are sufficient to bypass crystallization. These findings are relevant for an industrial scope, as commercial-grade purity feedstock material was used and still a fully amorphous state was obtained in the gas-atomized powder. The cooling rates during atomization are comparable to the transient cooling present during PBF-LB/M, suggesting a sufficient GFA to additively process amorphous samples [1,2].

In addition to cooling rates and rapid solidification, the glass formation depends on the purity of the alloy. A common and critical indicator for the impurity of BMGs is the presence of oxygen. Fig. 7 displays the oxygen uptake during atomization for the powders considering the initial oxygen level in the feedstock material (470 μg/g). The concentration in the feedstock was estimated on the basis of the weighted average calculated from the commercial purity degree of the individual elements (manufacturers information). In the spray chamber, the measured oxygen concentration is 100 ppm. Possible contamination of moisture is discarded as the powders were kept fully sealed in small volume sample glasses suitable for powder storage, inside a vacuum desiccator.

It is revealed that the different atomization parameters and microalloying with Si and Sn are unrelated to the oxygen content within the powder. Instead, a strong correlation with the particle size is found. The highest oxygen concentrations are present in the smallest particles, in which the uptake surpassed 1500 μg/g in some cases. In contrast, the coarser particles incorporate remarkably less oxygen. Hence, the results indicate the surface-to-volume ratio clearly governs the oxygen content. This is consistent with previous results reported for Vit101 gas-atomized powder [55–57]. The surface-to-volume effect controls the interaction of particles atomized under conventional cooling with oxygen as the gas-atomized powders experience slow oxidation posterior to the atomization in an inert gas atmosphere. As a consequence, an oxide film is formed on the surface [37], which depends on the chemistry of the alloy.

Moreover, the feedstock purity contributes to the initial oxygen content of the powder. For comparison, the oxygen concentration was measured in Cu-Ti feedstock prepared with high purity (HP) elements, as well as in commercial and high purity feedstocks for AMZ4. The high purity Cu-Ti feedstock contained 204 ± 28 μg/g of oxygen, which is less than half of the concentration present in the commercial purity material (470 μg/g as indicated in Fig. 7). For the AMZ4 alloy, the commercial purity feedstock contained 741 ± 22 μg/g oxygen, while the high purity feedstock 127 ± 37 μg/g. As anticipated, a much higher oxygen affinity for the Zr-based alloy was identified. Due to the lower affinity of copper to oxygen, it is therefore likely that commercial purities feedstocks are sufficient for processing Cu-Ti BMGs via PBF-LB/M. The volume chamber of the AM machines is smaller than the atomization spray chamber, so it is expected that the atmosphere can be more systematically controlled and the oxygen avoided. Thus, further research regarding the oxygen uptake during AM would be worthwhile to justify the economic viability of these alloys.

4. Summary

In the present study, processing properties of gas-atomized $Cu_{47}Ti_{34}Zr_{11}Ni_8$ (Vit101), $Cu_{47}Ti_{33}Zr_{11}Ni_8Si_1$ (Vit101Si), and $Cu_{47}Ti_{33}Zr_{11}Ni_6Sn_2Si_1$ (Vit101SiSn) glass-forming alloys were

investigated. The Cu-Ti-based system was selected due to its low-cost feedstock and high strength with adequate glass-forming capability desired for PBF-LB/M processability. Feedstock material using pure elements with commercial purity was used to account for broad applicability from an economic viewpoint. The atomization parameters were varied, in which the gas pressure and temperature were increased aiming for vitrification and a higher yield in the 20–63 μm powder class size.

It was shown that the Vit101, Vit101Si and Vit101SiSn alloys present similar particle size distribution when atomized under the same conditions. As expected, the increase of gas pressure and gas temperature produces finer particles. A positive consequence is the increased powder yield in the range of 20–63 μm, typical for additive manufacturing (AM) applications. The drawback of hot gas (HG) atomization is the increased formation of satellite particles. Because they remain attached to primary coarser particles, the particle shape factors of circularity and aspect ratio are overall reduced. It is also observed the generation of small particles (<20 μm) with HG. Nevertheless, the particles synthesized present a highly spherical shape and smooth surface. In addition, the flowability investigation indicates the powder is suitable for AM, but a strong influence of moisture uptake is observed. The Vit101SiSn alloy seems the most prone to moisturization, as the flow behavior rapidly deteriorated after short exposure to the environment.

The investigation of the crystalline state reveals that the gas-atomized powders at a particle class size of 20–63 μm are fully amorphous. X-ray powder diffraction and high-energy synchrotron radiation confirms the results. Given that commercial purity feedstocks were used, these findings positively contribute to the economic aspect of this alloy system in industrial applications. The amorphous solidification of the powder indicates a suitable GFA for the processability of the Cu-Ti-based metallic glasses via PBF-LB/M. Measurements of the oxygen content in the powder reveal the lack of influence of the atomization parameters and microalloying with Si and Sn. It was confirmed the oxygen uptake during atomization is a function of the particle size, as the surface-to-volume ratio governed the oxygen content.

Data Availability Statement

The raw/processed data required to reproduce these findings cannot be shared at this time as the data also forms part of an ongoing study.

Funding

This research was funded by the German Federal Ministry for Economic Affairs and Energy (BMWi) within the Promotion of Joint Industrial Research Programme (IGF) due to a decision of the German Bundestag. It was part of the research project 21227 N (LaSaM) by the Association for Research in Precision Mechanics, Optics and Medical Technology (F.O.M.) under the auspices of the German Federation of Industrial Research Association (AiF).

CRediT authorship contribution statement

Erika Soares Barreto: Conceptualization, Methodology, Investigation, Data curation, Writing – original draft, Visualization. **Maximilian Frey:** Methodology, Validation, Resources. **Jan Wegner:** Methodology, Validation, Formal analysis, Writing – review & editing. **Allen Jose:** Investigation, Data curation, Writing – review & editing. **Nico Neuber:** Investigation, Data curation, Writing – review & editing. **Ralf Busch:** Resources, Formal analysis, Supervision, Funding acquisition. **Stefan Kleszczynski:** Formal analysis, Supervision, Funding acquisition. **Lutz Mädler:** Formal analysis, Supervision, Writing – review & editing. **Volker Uhlenwinkel:** Conceptualization, Formal analysis, Supervision, Project administration, Funding acquisition.

Declaration of Competing Interest

The authors declare that they have no known competing financial interests or personal relationships that could have appeared to influence the work reported in this paper.

Acknowledgement

The authors would like to thank F. Peschel and S. Evers for their technical assistance, S. Schmidt for the chemical analysis, C. Mahnke for the microscopy analysis, and B. Adam and L. Ruschel for the assistance with the HESXRD measurements. We further acknowledge DESY (Hamburg, Germany), a member of the Helmholtz Association HGF, for the provision of experimental facilities. Parts of this research were carried out at PETRA III and we want to thank M. Blankenburg and U. Lienert for assistance in using the P21.2 beamline facility. Additionally, we further acknowledge the AiF project support committee for the project support and fruitful discussions during our meetings. We especially thank Dr. Blatter and the PX Group for the material provision for atomization.

Appendix A

See 1 Fig. A1 for the cumulative mass distribution Q_3 as a function of particle size of all as-atomized powders investigated in this study.

See Fig. B1 for chemical composition analysis of the powder obtained with EDX.

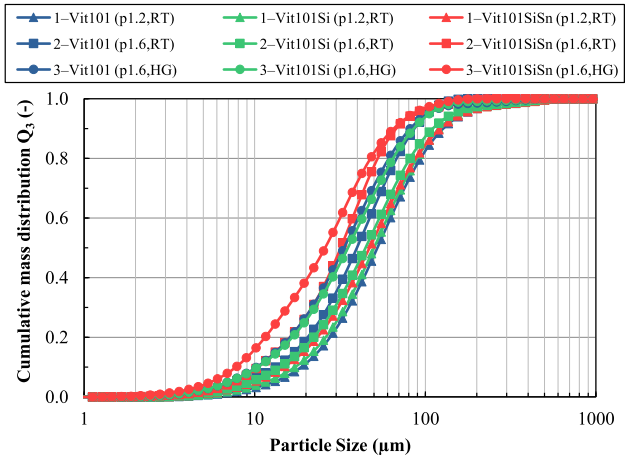

Fig. A1. Cumulative mass distribution Q3 as a function of particle size for the as-atomized powders. While the increase of gas pressure and gas temperature yielded finer powder, the chemical composition of the alloys had a lower influence on the particle size distribution. Due to powder losses caused by self-ignition of the Vit101SiSn powder, the results for Runs 2 and 3 were biased into finer distributions.

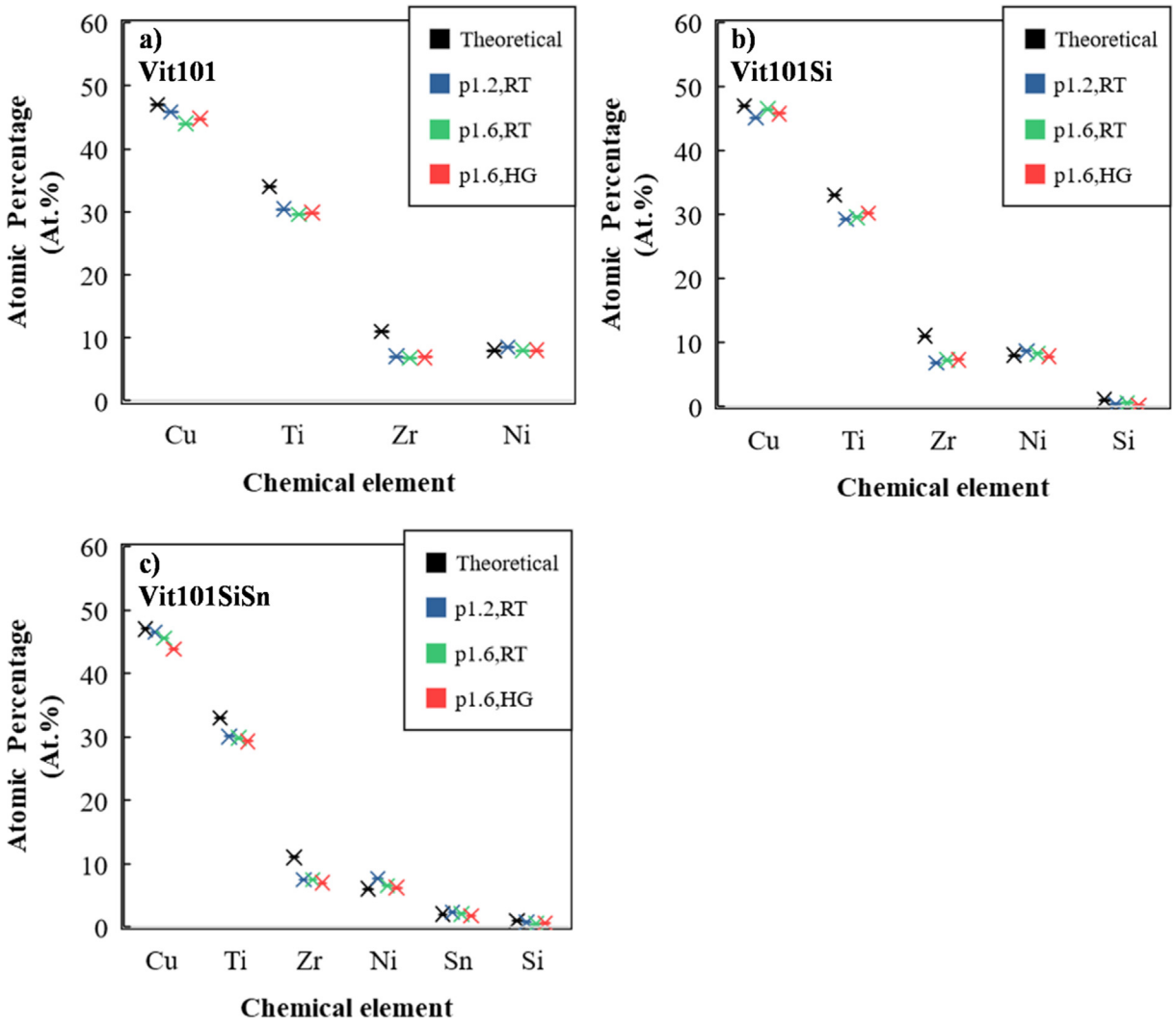

Fig. B1. Chemical composition analysis of the powder obtained with EDX in comparison to the theoretical chemical composition of the alloy.

References

[1] U. Scipioni Bertoli, G. Guss, S. Wu, M.J. Matthews, J.M. Schoenung, In-situ characterization of laser-powder interaction and cooling rates through high-speed imaging of powder bed fusion additive manufacturing, Mater. Des. 135 (2017) 385–396.

[2] N. Sohrabi, J. Jhabvala, R.E. Logé, Additive Manufacturing of Bulk Metallic Glasses—Process, Challenges and Properties: A Review, Metals 11 (8) (2021).

[3] H. Choi-Yim, R. Busch, W.L. Johnson, The effect of silicon on the glass forming ability of the Cu47Ti34Zr11Ni8 bulk metallic glass forming alloy during processing of composites, J. Appl. Phys. 83 (12) (1998) 7993–7997.

[4] S.C. Glade, The $Cu_{47}Ti_{34}Zr_{11}Ni_8$ glass-forming alloy : thermophysical properties, crystallization, and the effect of small alloying additions on the thermal stability Engineering and Applied Science, California Institute of Technology, 2001.

[5] S.C. Glade, R. Busch, D.S. Lee, W.L. Johnson, R.K. Wunderlich, H.J. Fecht, Thermodynamics of Cu47Ti34Zr11Ni8, Zr52.5Cu17.9Ni14.6Al10Ti5 and Zr57Cu15.4Ni12.6Al10Nb5 bulk metallic glass forming alloys, J. Appl. Phys. 87 (10) (2000) 7242–7248.

[6] E.S. Park, H.K. Lim, W.T. Kim, D.H. Kim, The effect of Sn addition on the glass-forming ability of Cu–Ti–Zr–Ni–Si metallic glass alloys, J. Non-Cryst. Solids 298 (2002) 15–22.

[7] G.R. Garrett, M.D. Demetriou, J. Chen, W.L. Johnson, Effect of microalloying on the toughness of metallic glasses, Appl. Phys. Lett. 101 (24) (2012).

[8] X.H. Lin, W.L. Johnson, Formation of Ti–Zr–Cu–Ni bulk metallic glasses, J. Appl. Phys. 78 (11) (1995) 6514–6519.

[9] S. Venkataraman, K. Biswas, On the fragility of Cu47Ti33Zr11Ni8Si1 metallic glass, J. Phys. D Appl. Phys. 39 (12) (2006) 2600–2608.

[10] A.B. Spierings, M. Voegtlin, T. Bauer, K. Wegener, Powder flowability characterisation methodology for powder-bed-based metal additive manufacturing, Prog. Addit. Manuf. 1 (1–2) (2015) 9–20.

[11] L. Haferkamp, L. Haudenschild, A. Spierings, K. Wegener, K. Riener, S. Ziegelmeier, G.J. Leichtfried, The Influence of Particle Shape, Powder Flowability, and Powder Layer Density on Part Density in Laser Powder Bed Fusion, Metals 11 (418) (2021).

[12] S. Vock, B. Klöden, A. Kirchner, T. Weißgärber, B. Kieback, Powders for powder bed fusion: a review, Prog. Addit. Manuf. 4 (4) (2019) 383–397.

[13] D. Beckers, N. Ellendt, U. Fritsching, V. Uhlenwinkel, Impact of process flow conditions on particle morphology in metal powder production via gas atomization, Adv. Powder Technol. 31 (1) (2020) 300–311.

[14] E. Gärtner, H.Y. Jung, N.J. Peter, G. Dehm, E.A. Jägle, V. Uhlenwinkel, L. Mädler, Reducing cohesion of metal powders for additive manufacturing by nanoparticle dry-coating, Powder Technol. 379 (2021) 585–595.

[15] U. Fritsching, Droplets and particles in sprays: tailoring particle properties within spray processes, China Particuol. 3 (1–2) (2005) 125–133.

[16] N. Ciftci, N. Ellendt, E. Soares Barreto, L. Mädler, V. Uhlenwinkel, Increasing the amorphous yield of {(Fe0.6Co0.4)0.75B0.2Si0.05}96Nb4 powders by hot gas atomization, Adv. Powder Technol. 29 (2) (2018).

[17] S. Hussain, C. Cui, L. He, L. Mädler, V. Uhlenwinkel, Effect of hot gas atomization on spray forming of steel tubes using a close-coupled atomizer (CCA), J. Mater. Process. Technol. 282 (2020).

[18] S. Pauly, C. Schricker, S. Scudino, L. Deng, U. Kühn, Processing a glass-forming Zr-based alloy by selective laser melting, Mater. Des. 135 (2017) 133–141.

[19] J.P. Best, H.E. Ostergaard, B. Li, M. Stolpe, F. Yang, K. Nomoto, M.T. Hasib, O. Muránsky, R. Busch, X. Li, J.J. Kruzic, Fracture and fatigue behaviour of a laser additive manufactured Zr-based bulk metallic glass, Addit. Manuf. 36 (2020).

[20] N. Luo, C. Scheitler, N. Ciftci, F. Galgon, Z. Fu, V. Uhlenwinkel, M. Schmidt, C. Körner, Preparation of Fe-Co-B-Si-Nb bulk metallic glasses by laser powder bed fusion: Microstructure and properties, Mater. Charact. 162 (2020).

[21] E. Soares Barreto, V. Uhlenwinkel, M. Frey, I. Gallino, R. Busch, A. Lüttge, Influence of Processing Route on the Surface Reactivity of Cu47Ti33Zr11Ni6Sn2Si1 Metallic Glass, Metals 11 (8) (2021).

[22] C.T. Liu, M.F. Chisholm, M.K. Miller, Oxygen impurity and microalloying effect in a Zr-based bulk metallic glass alloy, Intermetallics 10 (11–12) (2002) 1105–1112.
[23] I. Jonas, W. Hembree, F. Yang, R. Busch, A. Meyer, Industrial grade versus scientific pure: Influence on melt properties, Appl. Phys. Lett. 112 (17) (2018).
[24] A. Gebert, J. Eckert, L. Schultz, Effect of oxygen on phase formation and thermal stability of slowly cooled Zr65Al7.5Cu17.5Ni10 metallic glass, Acta Mater. 46 (15) (1998) 5475–5482.
[25] Z.P. Lu, H. Bei, Y. Wu, G.L. Chen, E.P. George, C.T. Liu, Oxygen effects on plastic deformation of a Zr-based bulk metallic glass, Appl. Phys. Lett. 92 (1) (2008).
[26] J. Wegner, M. Frey, M. Piechotta, N. Neuber, B. Adam, S. Platt, L. Ruschel, N. Schnell, S.S. Riegler, H.-R. Jiang, G. Witt, R. Busch, S. Kleszczynski, Influence of powder characteristics on the structural and the mechanical properties of additively manufactured Zr-based bulk metallic glass, Mater. Des. 209 (2021).
[27] M. Frey, J. Wegner, N. Neuber, B. Reiplinger, B. Bochtler, B. Adam, L. Ruschel, S. S. Riegler, H.-R. Jiang, S. Kleszczynski, G. Witt, R. Busch, Thermoplastic forming of additively manufactured Zr-based bulk metallic glass: A processing route for surface finishing of complex structures, Mater. Des. 198 (2021).
[28] X. Qiu, J.W. Thompson, S.J.L. Billinge, PDFgetX2: a GUI-driven program to obtain the pair distribution function from X-ray powder diffraction data, J. Appl. Crystallogr. 37 (4) (2004).
[29] H. Lubanska, Correlation of Spray Ring Data for Gas Atomization of Liquid Metals, JOM 22 (2) (1970) 45–49.
[30] H. Alain, Powder is the future of metallurgy, Euro PM2021 (2021).
[31] N. Ciftci, N. Ellendt, L. Mädler, V. Uhlenwinkel, Impact of hot gas atomization on glass forming alloys, World PM 2016, Hamburg, Germany, 2016.
[32] F. Chu, K. Zhang, H. Shen, M. Liu, W. Huang, X. Zhang, E. Liang, Z. Zhou, L. Lei, J. Hou, A. Huang, Influence of satellite and agglomeration of powder on the processability of AlSi10Mg powder in Laser Powder Bed Fusion, J. Mater. Res. Technol. 11 (2021) 2059–2073.
[33] H. Lohner, C. Czisch, P. Schreckenberg, U. Fritsching, K. Bauckhage, Atomization of Viscous Melts, Atomization Sprays 15 (2) (2005) 169–180.
[34] R. Busch, A. Masuhr, E. Bakke, W.L. Johnson, Bulk Metallic Glass Formation from Strong Liquids, Mater. Sci. Forum 269–272 (1998) 547–552.
[35] S.C. Glade, W.L. Johnson, Viscous flow of the Cu47Ti34Zr11Ni8 glass forming alloy, J. Appl. Phys. 87 (10) (2000) 7249–7251.
[36] M. Dopler, Influence of Material Properties on Spheroidisation of Gas Atomization Process, SSRN Electron. J. (2021).
[37] N. Ciftci, Cooling strategies for the atomization of glass-forming alloys, Department of Production Engineering, University of Bremen, 2020, p. 141.
[38] Z. Evenson, T. Schmitt, M. Nicola, I. Gallino, R. Busch, High temperature melt viscosity and fragile to strong transition in Zr–Cu–Ni–Al–Nb(Ti) and Cu47Ti34Zr11Ni8 bulk metallic glasses, Acta Mater. 60 (12) (2012) 4712–4719.
[39] R. Busch, The thermophysical properties of bulk metallic glass-forming liquids, JOM 52 (7) (2000) 39–42.
[40] S. Mukherjee, J. Schroers, Z. Zhou, W.L. Johnson, W.K. Rhim, Viscosity and specific volume of bulk metallic glass-forming alloys and their correlation with glass forming ability, Acta Mater. 52 (12) (2004) 3689–3695.
[41] R. Busch, J. Schroers, W.H. Wang, Thermodynamics and Kinetics of Bulk Metallic Glass, MRS Bull. 32 (8) (2011) 620–623.
[42] D. Hann, J. Stražišar, Influence of Particle Size Distribution, Moisture Content, and Particle Shape on the Flow Properties of Bulk Solids, Instrum Sci. Technol. 35 (5) (2007) 571–584.
[43] A. Mussatto, R. Groarke, A. O'Neill, M.A. Obeidi, Y. Delaure, D. Brabazon, Influences of powder morphology and spreading parameters on the powder bed topography uniformity in powder bed fusion metal additive manufacturing, Addit. Manuf. 38 (2021).
[44] M.Y. Shaheen, A.R. Thornton, S. Luding, T. Weinhart, The influence of material and process parameters on powder spreading in additive manufacturing, Powder Technol. 383 (2021) 564–583.
[45] A.A. Gokhale, G.W. Huber, J.A. Dumesic, M. Mavrikakis, Effect of Sn on the Reactivity of Cu Surfaces, J. Phys. Chem. B 108 (37) (2004) 14062–14073.
[46] L. Lefebvre, J. Dai, Y. Thomas, Y. Martínez-Rubí, Metal powder flowability: effect of humidity and impact on the reproducibility of the measurements, Additive Manufacturing with Powder Metallurgy, Metal Powder Industries Federation, Phoenix, USA, 2019.
[47] L. Cordova, T. Bor, M. de Smit, M. Campos, T. Tinga, Measuring the spreadability of pre-treated and moisturized powders for laser powder bed fusion, Addit. Manuf. 32 (2020).
[48] P. Mellin, M. Rashidi, M. Fischer, L. Nyborg, L. Marchetti, C. Hulme-Smith, M. Uhlirsch, A. Strondl, Moisture in Metal Powder and Its Implication for Processability in L-PBF and Elsewhere, BHM Berg- Huettenmaenn. Monatsh. 166 (1) (2021) 33–39.
[49] N. Ciftci, N. Ellendt, G. Coulthard, E. Soares Barreto, L. Mädler, V. Uhlenwinkel, Novel Cooling Rate Correlations in Molten Metal Gas Atomization, Metall. Mater. Trans. B 50 (2019).
[50] L. Deng, S. Wang, P. Wang, U. Kühn, S. Pauly, Selective laser melting of a Ti-based bulk metallic glass, Mater. Lett. 212 (2018) 346–349.
[51] B. Bochtler, M. Stolpe, B. Reiplinger, R. Busch, Consolidation of amorphous powder by thermoplastic forming and subsequent mechanical testing, Mater. Des. 140 (2018) 188–195.
[52] B. Bochtler, O. Kruse, R. Busch, Thermoplastic forming of amorphous metals, J. Phys.: Condens. Matter 32 (24) (2020) 244002.
[53] J. Schroers, Processing of bulk metallic glass, Adv. Mater. 22 (14) (2010) 1566–1597.
[54] T. He, N. Ciftci, V. Uhlenwinkel, S. Scudino, Synthesis of Bulk Zr48Cu36Al8Ag8 Metallic Glass by Hot Pressing of Amorphous Powders, J. Manuf. Mater. Process. 5 (1) (2021).
[55] D.J. Sordelet, E. Rozhkova, P. Huang, P.B. Wheelock, M.F. Besser, M.J. Kramer, M. Calvo-Dahlborg, U. Dahlborg, Synthesis of Cu47Ti34Zr11Ni8 Bulk Metallic Glass by Warm Extrusion of Gas Atomized Powders, J. Mater. Res. 17 (1) (2011) 186–198.
[56] D.J. Sordelet, E. Rozhkova, M.F. Besser, M.J. Kramer, Consolidation of gas atomized $Cu_{47}Ti_{34}Zr_{11}Ni_8$ amorphous powders, J. Non-Cryst. Solids 317 (1–2) (2003) 137–143.
[57] N. Ciftci, N. Yodoshi, S. Armstrong, L. Mädler, V. Uhlenwinkel, Processing soft ferromagnetic metallic glasses: on novel cooling strategies in gas atomization, hydrogen enhancement, and consolidation, J. Mater. Sci. Technol. 59 (2020) 26–36.